

The molecular gas in HE 0450-2958: fueling an AGN and a starburst apart

Padeli P. Papadopoulos¹

Argelander-Institut für Astronomie, Auf dem Hügel 71, D-53121 Bonn, Germany

padeli@astro.uni-bonn.de

Ilana J. Feain

CSIRO Australia Telescope National Facility, P.O. Box 76, Epping, NSW 1710, Australia

Ilana.Feain@CSIRO.AU

Jeff Wagg

NRAO, PO Box 0, Socorro, New Mexico, 87801, USA

jwagg@nrao.edu

and

David J. Wilner

Harvard-Smithsonian Center for Astrophysics, Cambridge, MA, 02138, USA

dwilner@cfa.harvard.edu

ABSTRACT

We report on interferometric observations of the CO J=1–0 and J=3–2 line emission from the controversial QSO/galaxy pair HE 0450–2958. *The detected CO J=1–0 line emission is found associated with the disturbed companion galaxy not the luminous QSO*, and implies $M_{\text{gal}}(\text{H}_2) \sim (1 - 2) \times 10^{10} M_{\odot}$, which is $\gtrsim 30\%$ of the dynamical mass in its $\sim 11 \text{ kpc} \times 6 \text{ kpc}$ CO-luminous region. Fueled by this large gas reservoir this galaxy is the site of an intense starburst with $\text{SFR} \sim 370 M_{\odot} \text{ yr}^{-1}$, placing it firmly on the upper gas-rich/star-forming end of Ultra Luminous Infrared Galaxies (ULIRGs, $L_{\text{IR}} > 10^{12} L_{\odot}$). This makes

¹Institut für Astronomie, ETH Zurich, 8093 Zürich, Switzerland

HE 0450–2958 the first case of extreme starburst and powerful QSO activity, intimately linked (triggered by a strong interaction) but not coincident. The lack of CO emission towards the QSO itself renews the controversy regarding its host galaxy by making a gas-rich spiral (the typical host of Narrow Line Seyfert 1 AGNs) less likely. Finally, the prominence of HE 0450–2958 and similar IR-warm QSOs as ULIRG→QSO transition candidates raises the possibility that some may *simply be gas-rich/gas-poor (e.g. spiral/elliptical) galaxy interactions* “activating” an optically bright unobscured QSO in the gas-poor galaxy, and a starburst in the gas-rich one. We argue that such events may have gone largely unnoticed even in the local Universe because the tools necessary to disentangle the progenitors, namely the combination of high S/N optical and CO imaging at high resolution, became available only recently.

Subject headings: galaxies: active — galaxies: ISM — galaxies: starburst — ISM: molecules — quasars: individual (HE 0450-2958) — galaxies: mergers

1. Introduction

HE 0450-2958 is an optically bright ($M_v = -25.8$), IR-selected, QSO at a redshift of $z=0.286$, with a warm $25\mu\text{m}/60\mu\text{m}$ color ratio (~ 0.25), a criterion that efficiently selects dust-enshrouded AGNs among the IR-bright galaxies discovered by *IRAS* by identifying the AGN-heated dust component (de Grijp, Miley, & Lub 1987). It was spectroscopically confirmed as a QSO by Low et al. (1988), and its complex environment, marked by tidal interactions, was identified early with ground-based (Hutchings, & Neff 1988) and *HST* imaging (Boyce et al. 1996). All these efforts revealed a strongly interacting system consisting of the QSO and a disturbed galaxy $\sim 1.5''$ away, setting this QSO/galaxy pair on par with typical Ultra Luminous Infrared Galaxies (ULIRGs) in terms of morphology as well as IR luminosity ($L_{\text{IR}} \sim 5 \times 10^{12} L_{\odot}$). The scarcity of such IR *and* optically luminous QSOs made HE 0450-2958 an early favorite candidate undergoing a ULIRG→(optically bright QSO) transition (e.g. Hutchings, & Neff 1988; Canalizo & Stockton 2001) in the scenario proposed by Sanders et al. 1988. In this picture mergers of two gas-rich progenitors induce a starburst and an AGN lying *within* heavily dust-obscured environments. As star-formation uses and disperses the large molecular gas/dust reservoirs of ULIRGs, their initially cool dust emission SED changes towards one dominated by the warm AGN-heated dust (and hence towards warm IR colors) and eventually an unobscured optically bright QSO emerges.

HE 0450-2958 acquired singular significance when Magain et al. (2005), after carefully subtracting the AGN emission from an ACS/HST image, failed to find the QSO host galaxy

expected from well-established and tight (host galaxy)-quasar correlations of properties (e.g. McLure & Dunlop 2002; Floyd et al. 2004). This potentially pivotal result has been upheld by independent analysis (Kim et al. 2007), and follow-up VLT spectroscopic observations weakened the hypothesis of a significantly dust-enshrouded QSO host galaxy (Letawe et al. 2007). The possibility of an ejected (black-hole)+(accretion disk) system as responsible for a “naked” QSO, its serious consequences and other observable signatures have been discussed in several papers. Summarizing their results here, such a QSO could be produced either by a Newtonian three-body “kick” exerted on a lighter black hole by a black hole binary residing in a gas-poor elliptical (Haehnelt, Davies, & Rees 2005; Hoffman & Loeb 2006), or by the recoil of a coalesced binary of spinning black holes due to an asymmetric gravitational wave emission (Haehnelt et al. 2005; Loeb 2007). The stage for both scenarios demands a strong galaxy interaction, and both have important consequences for the detection of gravitational waves by future gravity wave detectors such as *LISA*, and the hierarchical build-up of supermassive black holes in galaxy centers (Haehnelt et al. 2005 and references therein).

In the present work we report on the detection and imaging of CO J=1–0, the prime molecular line used to trace metal-rich H₂ gas in galaxies, and place a sensitive limit on the luminosity of the J=3–2 transition using the Australian Telescope Compact Array (ATCA), and the Smithsonian Submillimeter Array Array (SMA) respectively. We then discuss implications for the nature of HE 0450-2958, the prevailing views regarding galaxy interactions, and the so called ULIRG→QSO transition objects. We adopt a cosmology with $H_0 = 71 \text{ km s}^{-1} \text{ Mpc}^{-1}$, $\Omega_M = 0.27$ and $\Omega_\Lambda = 0.73$, for which the luminosity distance of HE 0450-2958 at $z=0.286$ is $D_L = 1460.4 \text{ Mpc}$ and $1'' \rightarrow 4.28 \text{ kpc}$.

2. Observations

We used the ATCA to image the CO J=1–0 line emission ($\nu_{\text{rest}} = 115.2712 \text{ GHz}$) towards the QSO/galaxy system HE 0450-2958 during four periods in April, August 2006 and May, August 2007 utilizing its hybrid H 214 and H 168 configurations that enable full uv coverage. For the mean redshift $z = 0.2864$ of the pair (Canalizo & Stockton 2001), the CO line is redshifted to $\nu(z) = 89.608 \text{ GHz}$, well within the tuning range of ATCA’s 3 mm receivers (available in 5 of the 6 antennas). The correlator setup consisted of two IF modules of $64 \times 2 \text{ MHz}$ channels each, and frequency resolution of $\Delta\nu_{\text{res}} \sim 2.2\Delta\nu_{\text{ch}} = 4.4 \text{ MHz}$ over an effective velocity coverage of $V_{\text{IF1+IF2}} \sim (-300 \rightarrow +270) \text{ km s}^{-1}$ (after flagging bad edge channels and channel overlap between the IF modules). Pointing was checked hourly, and typical offsets were $\sim 5''$ (rms), while the field of view of ATCA antennas at this frequency is $32''$ (HPBW). The array phase center was placed at the AGN’s position marked by its radio

core at 8.6 GHz (C1 component in Feain et al. 2007). Dedicated wideband mm continuum observations were conducted using the two IFs in series tuned around a center frequency ~ 94.53 GHz (well away from the CO line), and the same array configurations (two tracks with H 214, three tracks with H 168). For the mm continuum observations the phase center was placed one synthesized beam away from the QSO itself as to avoid any (highly unlikely) small correlator DC offsets masking as a weak continuum source at the phase center. Typical system temperatures during all observing sessions were $T_{\text{sys}} \sim (200 - 350)$ K (including atmospheric absorption), estimated with hourly vane calibration performed per antenna.

During all observing periods amplitude/phase calibration was obtained with observations of 0454-234 interleaved with the program source in 1min/(3-5)mins calibrator/source intervals, and passband calibration was achieved by observing 1921-293 or 2223-052. The absolute flux scale of the visibilities was set by bootstrapping the flux of 0454-234 using observations of Uranus and/or Mars taken at each track, and its uncertainty of $\sim 15\%$ was estimated from the observed dispersion of the amplitudes of the various calibrators.

2.1. The SMA observations

A search for the redshifted CO J=3–2 line emission ($\nu_{\text{rest}} = 345.796$ GHz) was also conducted using the 8-element SMA¹ interferometer on 2006 Dec. 9 with a median atmospheric opacity at 225 GHz of $\tau_{225} \sim 0.08$. This transition is redshifted to 269.102 GHz, where the lower sideband (LSB) of the 345 GHz receivers could be placed, with a bandwidth of 1.968 GHz ($\sim 2200 \text{ km s}^{-1}$). The array was in its extended configuration, resulting in a synthesized beam of $\sim 1''.20 \times 0''.94$, PA=16.9° at the observed frequency and the uv coverage attained. The mean system temperature was $T_{\text{sys}} = 490$ K (DSB), and the total on-source integration time ~ 5.07 hrs. Calibration of the antenna gain variations was done by observing the nearby calibrators 0522-364 and 0455-462, at regular 10 minute intervals. Saturn and 3C454.3 were used to calibrate the bandpass, while Uranus was observed for flux calibration, with an expected uncertainty of $\sim 20\%$. The MIR package was then used for the calibration of the visibility data. A search for 275 GHz continuum yielded an upper limit of $S_{275 \text{ GHz}} \leq 8 \text{ mJy/beam}$ (3σ), over a ~ 3.936 GHz bandwidth (both sidebands).

¹The Submillimeter Array is a joint project between the Smithsonian Astrophysical Observatory and the Academia Sinica Institute of Astronomy and Astrophysics and is funded by the Smithsonian Institution and the Academia Sinica.

3. Data reduction, imaging, and analysis

We used the *in-situ* ATCA phase monitor operating on a 230 m east-west baseline (Midelberg, Sault, & Kesteven 2006) to identify the periods when atmospheric phase noise at 90 GHz over this baseline (comparable to the longest ones in our dataset) exceeded $\sim 30^\circ$ (rms) and rejected the corresponding data. We then edited the remaining visibilities for temporal amplitude/phase jumps and the final uv dataset has a phase rms of $\sigma_\phi \sim 20^\circ$, in accordance with a mean coherence factor $\rho_{\text{coh}} = \langle V(u, v) \rangle / S = e^{-\sigma_\phi^2(\text{rad})/2} \sim 0.95$ or better (estimated after imaging the calibrator data with an assumed flux of unity, and antenna gains smoothed by $T_{\text{avg}} \sim 2 \times T_{\text{cycle}}(\text{QSO} \leftrightarrow \text{calibrator}) \sim 12$ mins).

Imaging was done using MIRIAD’s task INVERT with natural weight used in all maps for maximum sensitivity. CO J=1–0 emission is detected independently with both H 214 and H 168 array datasets with peak flux densities differing by $\sim 15\%$, consistent with the flux calibration uncertainties. The CO J=1–0 emission map was produced by multi-frequency synthesis using the entire on-the-line IF1+IF2 band and after combining both configurations. Deconvolution with the Clark algorithm was also performed and the resulting map along with the CO spectrum from the peak brightness position is shown in Figure 1, while the mm continuum of the same region where no such emission is detected is shown in Figure 2.

3.1. Characteristics of the CO J=1–0 emission region

Our high S/N detection allows a robust determination of the position of the peak CO brightness $S_{\text{peak}} = 6.7 \text{ mJy/beam}$ ($S/N \sim 15$ for $\sigma_{\text{rms}} = 0.45 \text{ mJy/beam}$) as well as the source size and total flux (if extended). Using the MIRIAD task IMFIT to fit a gaussian source model we obtain $(\Delta\alpha, \Delta\delta) = (1.15'' \pm 0.12'', -1.05'' \pm 0.10'')$ for the position of peak brightness relative to the phase center, a deconvolved source size of $\sim 2.5'' \times 1.5''$ ($\text{PA} = 35^\circ \pm 10^\circ$), and a total flux density of $S_\nu^{(\text{tot})}(\text{CO}) = (10 \pm 2) \text{ mJy}$. The latter is similar to the total CLEANed flux from the source region and accounts for all the CO flux density of the QSO/galaxy pair (i.e. the noise over the source region in the residual image after subtraction of the model is $\sigma_{\text{res}} \sim \sigma_{\text{rms}} \sim 0.45 \text{ mJy/beam}$). Fitting images of the secondary calibrator 0454-234, produced with $T_{\text{avg}} = (1 - 12) \text{ mins}$ of averaging interval of antenna gain solutions yield seeing disks of $\sim 0.30'' - 0.45''$, consistent with the expected size of $\Delta\theta_{\text{seeing}} \sim [\sigma_\phi(\text{rad})/2\pi]\sqrt{8\ln 2} \langle \Theta_{\text{beam}} \rangle \sim 0.34''$ (for $\sigma_\phi \sim 20^\circ$ and $\langle \Theta_{\text{beam}} \rangle = \sqrt{\Theta_1 \Theta_2} \sim 2.62''$), and much smaller than the deduced size of the CO emission region.

The aforementioned positional uncertainties of the peak brightness position *relative* to the phase center (placed at the QSO’s radio core) are those expected from a finite S/N,

namely $\delta\theta_{\text{rms}} \sim 1/2 \langle \Theta_{\text{beam}} \rangle (S/N)^{-1} \sim 0.09''$. The angular proximity of the amplitude/phase calibrator to the program source ($|\Delta\vec{k}| \sim 6.5^\circ$) allows for good absolute astrometry by limiting the uncertainty $\delta\theta_{\text{bas}} = (\delta\vec{B} \cdot \Delta\vec{k})/B \approx (\delta\phi_{\text{bas}}/2\pi)\langle \Theta_{\text{beam}} \rangle$ due to the phase error $\delta\phi_{\text{bas}} \sim (2\pi/\lambda)(\delta\vec{B} \cdot \Delta\vec{k})$ caused by baseline calibration uncertainties ($\sim |\delta\vec{B}|/B$). For a typical baseline length uncertainty of $|\delta\vec{B}| = \delta x_{\text{mm}} \sim 1 \text{ mm}$, it is $\delta\theta_{\text{bas}} \sim 0.086(\delta x_{\text{mm}})'' \sim 0.086''$.

4. The molecular gas and dust in HE 0450–2958

The CO J=1–0 emission overlaid with the 8.4 GHz radio continuum is shown in Figure 3 where a good correspondence with the radio emission region C2 associated with the companion galaxy (Feain et al. 2007) is evident. The deconvolved CO(1–0) source model, overlaid with the HST/ACS optical image of HE 0450–2958 in Figure 4, further underlines its association with the companion galaxy $\sim 1.56'' \pm 0.18''$ (6.7 kpc) away from the QSO’s radio position), in terms of position, overall size, and orientation angle.

The corresponding H_2 mass is given by $M(\text{H}_2) = X_{\text{CO}} L_{\text{CO}(1-0)}$, where $L_{\text{CO}(1-0)} = \int_{\Delta V} \int_{A_s} T_b da dV$ is the velocity/area-integrated brightness temperature of the line at the source reference frame, and X_{CO} (in $M_\odot (\text{K km s}^{-1} \text{ pc}^2)^{-1}$ units) is the CO- H_2 luminosity-mass conversion factor. Using standard derivations (e.g. Solomon et al. 1997) we have

$$L_{\text{CO}(1-0)} = 3.25 \times 10^7 (1+z)^{-1} \left(\frac{\nu_{\text{co,rest}}}{\text{GHz}} \right)^{-2} \left(\frac{D_L}{\text{Mpc}} \right)^2 \left(\frac{I_{\text{CO}(1-0)}}{\text{Jy km s}^{-1}} \right) \text{K km s}^{-1} \text{pc}^2, \quad (1)$$

which for the line-integrated flux density of $I_{\text{CO}(1-0)} = (5.7 \pm 1.15) \text{ Jy km s}^{-1}$ yields $L_{\text{CO}(1-0)} = (2.3 \pm 0.46) \times 10^{10} \text{ K km s}^{-1} \text{ pc}^2$. The latter is close to the maximum CO luminosity observed for starbursts, beyond which it remains constant across redshift (Frayser et al. 1999; Evans, Surace, & Mazzarella 2000), a possible indication of a self-regulating process occurring in extreme (maximal?) starbursts. Using $X_{\text{CO}} \sim 1$ as the value more appropriate for such galaxies (Downes & Solomon 1998), we obtain $M(\text{H}_2) \sim 2.3 \times 10^{10} M_\odot$, *which places the companion galaxy in this galaxy/QSO pair firmly in the ULIRG category*, and at its most gas-rich upper end, similar to starbursts found at high redshifts (e.g. Greve et al. 2005).

A lower limit in the H_2 gas mass can be obtained by assuming that the ^{12}CO J=1–0 emission is optically thin. Using the derivation in Bryant & Scoville 1996 and assuming LTE, the new conversion factor becomes

$$\frac{M(\text{H}_2)}{L_{\text{CO}(1-0)}} \sim 0.08 \left(\frac{[\text{CO}/\text{H}_2]}{10^{-4}} \right)^{-1} \left[\frac{g_1}{Z} e^{-T_o/T_k} \left(\frac{J(T_k) - J(T_{\text{bg}})}{J(T_k)} \right) \right]^{-1} \frac{M_\odot}{\text{K km s}^{-1} \text{pc}^2}, \quad (2)$$

where $T_o = E_1/k_B \sim 5.5 \text{ K}$, $J(T) = T_o (e^{T_o/T} - 1)^{-1}$, $T_{\text{bg}} = (1+z)T_{\text{cmb}} \sim 3.5 \text{ K}$, $g_1 = 3$, $Z \sim 2(T_k/T_o)$ (partition function), and $[\text{CO}/\text{H}_2] \sim 10^{-4}$ (for solar metallicity). For typical star-forming gas $T_k \sim 40 - 60 \text{ K}$, the last equation yields $\langle X_{\text{CO}}^{(\text{thin})} \rangle_{T_k} \sim 0.55 M_\odot (\text{K km s}^{-1} \text{pc}^2)^{-1}$, and thus $M(\text{H}_2)_{\text{min}} \sim 1.25 \times 10^{10} M_\odot$.

The mm/IR dust continuum SED of HE0450–2958 (Figure 5) is typical of the warm ULIRGs where the presence of warm dust was the prime reason they were considered as ULIRG \rightarrow QSO transition objects in the typical evolutionary scenario linking these two classes. Two-component fitting yields $T_{\text{dust}}^{(\text{cool})} = 45 - 55 \text{ K}$ and $T_{\text{dust}}^{(\text{warm})} \sim 175 - 194 \text{ K}$ (for emissivities of $\beta = 1 - 2$). Adopting $\beta = 1.5$ as our working value yields $T_{\text{dust}}^{(\text{cool})} = 48 \text{ K}$, $M_{\text{dust}}^{(\text{cool})} \sim 10^8 M_\odot$, and corresponds to $L_{\text{FIR}} = 2.1 \times 10^{12} L_\odot$. The warm AGN-residing dust has $T_{\text{dust}}^{(\text{warm})} = 184 \text{ K}$, $M_{\text{dust}}^{(\text{warm})} \sim 5 \times 10^4 M_\odot$ with $L_{\text{mid-IR}} = 2.6 \times 10^{12} L_\odot$ but unlike the typical scenario this dust mass resides *outside* the companion galaxy containing the bulk of the molecular gas and cooler dust mass. Indeed, assuming the cooler dust mass residing solely in the companion galaxy yields $M(\text{H}_2)/M_{\text{dust}}^{(\text{cool})} \sim 125 - 230$. This is well within the range expected for the gas/dust ratios in IRAS galaxies (e.g. Sanders, Scoville, & Soifer 1991), thus adding confidence to this spatial decomposition of the dust emission SED of this galaxy/QSO interacting pair. A starburst in the gas-rich galaxy would then be the natural source of its large far-IR luminosity, which in turn implies a star formation rate of $\text{SFR} \sim 1.76 \times 10^{-10} (L_{\text{IR}}/L_\odot) M_\odot \text{yr}^{-1} \sim 370 M_\odot \text{yr}^{-1}$ with an efficiency of $\text{SFE} \sim L_{\text{FIR}}/M(\text{H}_2) \sim (90 - 165) (L_\odot/M_\odot)$. These are typical values for ULIRGs, with SFE well below the maximum value $\sim 500 (L_\odot/M_\odot)$, expected from O, B star radiation-regulated feedback (Scoville 2004). Regarding the QSO itself, subtraction of the CO source model leaves no residual line emission in its location with $S_{\text{gal}}^{(\text{peak})}/S_{\text{QSO-host}} \gtrsim 5 (3\sigma)$, which corresponds to $M_{\text{gal}}(\text{H}_2)/M_{\text{QSO-host}}(\text{H}_2) \gtrsim 5 : 1$ (for a common velocity range and X_{CO} value).

The results above are certainly in good accord with evidence of significant star formation and reddening in the companion galaxy and no such activity or dust obscuration evident in a putative QSO host galaxy (Magain et al. 2005; Letawe, Magain, & Courbin 2007). They contradict the recent view espoused by Kim et al. 2007 regarding the nature of the companion galaxy, and set HE0450–2958 apart from typical ULIRGs with double nuclei. The latter have molecular gas mass ratios of $\sim 1 : 1 - 2 : 1$ (Sanders & Ishida 2004; Evans, Surace, & Mazzarella 2000), and their AGNs (when present) reside in the most gas-rich member of the interacting/merger pair (e.g. Evans et al. 1999, 2002). However we must bear in mind that a different (higher) X_{CO} factor applicable for the molecular gas in the QSO

host can reduce the aforementioned asymmetry in molecular gas mass distribution, while CO emission could be at the QSO’s location but at velocities outside our velocity coverage of $\sim 570 \text{ km s}^{-1}$. The latter possibility is rather small, given the similar systemic velocities of the ULIRG, the QSO, and the highly excited ionized gas next to it (Merritt et al. 2006).

4.1. Limits on the molecular gas excitation

The CO J=3–2 observations yielded a 3σ upper limit of $I_{\text{CO}(3-2)} \lesssim 3N_b^{1/2} \delta S_{\text{CO}(3-2)} \Delta V$, where $\delta S_{\text{CO}(3-2)} \sim 6.6 \text{ mJy/beam}$ is the noise of the CO J=3–2 map, $N_b \sim 3.3$ is the number of SMA beams corresponding to the CO J=1–0 emitting region (Section 3.1) and $\Delta V \sim 570 \text{ km s}^{-1}$ the velocity range of the two maps. This yields $I_{\text{CO}(3-2)} \lesssim 20 \text{ Jy km s}^{-1}$, and a line luminosity $L_{\text{CO}(3-2)} \lesssim 9 \times 10^9 \text{ K km s}^{-1} \text{ pc}^2$ (using Equation 1). This corresponds to a (3–2)/(1–0) brightness temperature ratio of $R_{32} \lesssim 0.39$, which is somewhat low for starburst related gas where $\langle R_{32} \rangle \sim 0.65$ (e.g. Devereux et al. 1994; Yao et al. 2003). An extensive $[n(\text{H}_2), T_{\text{kin}}, \Lambda_{\text{CO}}]$ grid of models with our Large Velocity Gradient (LVG) code ($\Lambda_{\text{CO}} = [\text{CO}/\text{H}_2]/(dV/dR)$, and $[\text{CO}/\text{H}_2] \sim 10^{-4}$ for metal-rich environments), restricted by the condition of $T_{\text{kin}} \geq T_{\text{dust}} \gtrsim 50 \text{ K}$ (the gas cools less efficiently than dust and turbulent/photoelectric heating heat the gas much more than the dust), yields wide swaths of the parameter space reproducing this ratio. However all have $n(\text{H}_2) \sim (10^2 - 10^3) \text{ cm}^{-3}$ which are rather low densities for star-forming gas ($n(\text{H}_2) \gtrsim 10^4 \text{ cm}^{-3}$) and more consistent the presence of a diffuse, warm gas phase frequently found in ULIRGs (e.g. Aalto et al. 1995; Downes & Solomon 1998). The lowest ratio $R_{32}^{(\text{min})} \sim 0.22$ found in LIRGs (Yao et al. 2003) suggests that deeper SMA observations of CO J=3–2 at a lower resolution that better matches the CO J=1–0 source size should eventually detect the J=3–2 line in HE 0450–2958 and shed light on the average physical conditions of its molecular gas.

4.2. The dynamical mass of the companion starburst galaxy

The line profile towards the peak CO emission shows signs of a rotating disk (Figure 1), though the poorer S/N per channel across the band makes this far from certain, and e.g. two independently moving gaseous reservoirs are also possible. The CO source model shows good overall agreement with the galaxy’s optical image (Figure 4), and at $z = 0.2864$: $2.5'' \times 1.5'' \rightarrow 10.7 \text{ kpc} \times 6.4 \text{ kpc}$, dimensions comparable to those of CO-bright regions in typical spiral disks (Regan et al. 2001; Helfer et al. 2003), including the Milky Way, but with $\sim 10 - 20$ times more H_2 gas mass.

For an underlying disk geometry the source angular dimensions correspond to an inclination angle $\cos i = \theta_{\text{minor}}/\theta_{\text{major}} = 0.6 \Rightarrow i \sim 53^\circ$. The enclosed dynamical mass then is

$$M_{\text{dyn}} \sim \frac{R}{G} \left(\frac{V_{\text{rot}}^{(\text{obs})}}{\sin i} \right)^2 \sim 2.32 \times 10^5 \left(\frac{R}{\text{kpc}} \right) \left(\frac{V_{\text{rot}}^{(\text{obs})}/\sin i}{\text{km s}^{-1}} \right)^2 M_{\odot}, \quad (3)$$

and for $R \sim R_{\text{major}}/2 \sim 5.35 \text{ kpc}$, $V_{\text{rot}}^{(\text{obs})} = (100 - 150) \text{ km s}^{-1}$ yields $M_{\text{dyn}} \sim (1.9 - 4.4) \times 10^{10} M_{\odot}$. Thus the galaxy’s molecular gas mass amounts to $\gtrsim 30\%$ of the dynamical mass enclosed in the CO-emitting region, making this ULIRG a very gas-rich system.

5. Implications for the QSO’s host galaxy

The disturbed nature of the HE 0450-2958 system and the extreme starburst in the gas-rich companion galaxy $\sim 6.5 \text{ kpc}$ away from the QSO solidifies a strong interaction as the necessary framework for its interpretation. A proposition that the AGN in this system shares many properties with Narrow Line Seyfert 1 (NLSy1) AGNs that have lower mass black holes was made by Merrit et al. (2006) in order to reconcile the lack of a massive spheroid reported by Magain et al. (2005). However this rests on the weak premise of a good analogy between luminous QSOs (usually hosted by massive gas-poor ellipticals) and the much less luminous Seyfert galaxies (usually gas-rich spirals), while not considering the results of another approach using well-established *empirical* AGN-(host galaxy) correlations that lead towards the same perplexing conclusions (Magain et al. 2005).

Indeed NLSy1 AGNs are typically hosted by gas-rich spirals with luminous starbursts, while optically luminous QSOs with $M_V < -24$ reside mostly in gas-poor massive elliptical hosts (Floyd et al. 2004). For example in I Zw 1 (the closest QSO and a prototypical NLSy1), a spiral disk hosts a massive circumnuclear starburst at a radius of $\sim 1.9 \text{ kpc}$ (Schinnerer, Eckart, & Tacconi 1998; Staguhn et al. 2004) fueled by a large molecular gas reservoir. None of that is evident in the vicinity of the AGN in the HE 0450-2958 system whose bulk of the molecular gas and starburst activity are found in the companion galaxy instead. Indicatively, at $z \sim 0.286$ our CO 1–0 observations could detect the molecular gas mass of the ~ 10 times less far-IR luminous I Zw 1 at a $S/N \sim 5$.

5.1. The AGN-bound gas and dust

Our spatial decomposition of the dust continuum emission SED with an AGN-heated dust mass of $\sim 5 \times 10^4 M_\odot$ corresponds to $M_{\text{AGN}}(\text{H}_2) \sim (0.6 - 1.15) \times 10^7 M_\odot$ (using the same gas/dust ratio as in the nearby ULIRG). This constitutes the first lower limit placed on the QSO’s host galaxy mass, albeit a weak one, and amounts to the mass of a few Giant Molecular Clouds (its emission well below the CO 1–0 upper limit for the AGN’s location). Similar amounts are found near AGNs that reside in galaxies such as NGC 1068 where $M(\text{H}_2)_{\text{AGN}} \sim 1.6 \times 10^7 M_\odot$ (for $X_{\text{CO}} = 1$) within ~ 70 pc of its AGN (Planesas, Scoville, & Myers 1991; Schinnerer, Eckart, & Tacconi 1999).

Given that this gas and dust reservoir is expected to partly obscure the AGN giving rise to the observed warm IR colors, a lower limit on the mass of the black hole can be set from

$$L_{\text{IR}}^{(\text{AGN})} = \frac{4\pi c G m_{\text{H}} f_{\text{c}} \epsilon_{\text{Edd}} M_{\text{BH}}}{\sigma_{\text{T}}} = 3.3 \times 10^{12} f_{\text{c}} \epsilon_{\text{Edd}} \left(\frac{M_{\text{BH}}}{10^8 M_\odot} \right) L_\odot, \quad (4)$$

where $f_{\text{c}} = L_{\text{IR}}^{(\text{AGN})}/L_{\text{AGN}} \leq 1$ is the fraction of the AGN’s intrinsic luminosity intercepted by the dust and re-radiated at IR wavelengths, and $\epsilon_{\text{Edd}} = L_{\text{AGN}}/L_{\text{Edd}}$ (L_{Edd} is the Eddington luminosity limit). Since $L_{\text{IR}}^{(\text{AGN})} = 2.6 \times 10^{12} L_\odot$, the last relation yields,

$$M_{\text{BH}} \sim 0.8(f_{\text{c}} \epsilon_{\text{Edd}})^{-1} 10^8 M_\odot. \quad (5)$$

For $\epsilon_{\text{Edd}} \sim 0.8$ (typical for $M_{\text{V}}(\text{QSO}) < -25$, Floyd et al. 2004) and $f_{\text{c}} \sim 0.71$ (estimated from $f_{\text{c}} = (1 + R_{\text{opt,IR}})^{-1}$ and setting $R_{\text{opt,IR}} = (L_{\text{opt}}/L_{\text{IR}})_{\text{AGN}} \sim [\nu_{\text{B}} f_{\nu}^{(\text{AGN})}(\text{B})]/[\nu_{60\mu\text{m}} f_{\nu}^{(\text{AGN})}(60\mu\text{m})] \sim 0.4$, Canalizo & Stockton 2001), it is $M_{\text{BH}} \sim 1.4 \times 10^8 M_\odot$.

Apart from partly obscuring the AGN in HE 0450-2958 the molecular gas mass inferred for its vicinity can in principle “fuel” it for

$$T_{\text{fuel}} = \frac{M_{\text{AGN}}(\text{H}_2)}{L_{\text{AGN}}/(c^2 \epsilon_{\text{BH}})} \sim 1.4 \times 10^8 \epsilon_{\text{BH}} f_{\text{c}} \left(\frac{L_{\text{IR}}^{(\text{AGN})}}{10^{12} L_\odot} \right)^{-1} \left[\frac{M_{\text{AGN}}(\text{H}_2)}{10^7 M_\odot} \right] \text{ yrs}, \quad (6)$$

where ϵ_{BH} is the black hole fuelling efficiency. For a typical $\epsilon_{\text{BH}} \sim 0.1$ and the deduced $M_{\text{AGN}}(\text{H}_2)$ the latter yields $T_{\text{fuel}} \sim (2.2 - 4.3) \times 10^6$ yrs. However unlike the molecular gas near (i.e. $r \leq 100$ pc) AGNs lying within H_2 -rich galaxies (e.g. Schinnerer et al. 1999), for HE 0450-2958 where the AGN lies well outside the only identified galaxy in the field, the origin of its H_2 gas reservoir is much less clear. The scenario of an ejected black hole places a

constraint on the maximum gas mass that can be carried off with it (while responsible for its observability at optical and IR wavelengths via fueling it and partly obscuring its activity). Following Loeb 2007, the recoiling remnant of a coalesced black hole binary can carry with it a gas disk with a mass

$$M_{\text{disk}} \sim 3 \times 10^5 \alpha^{-0.8} \eta^{-0.6} \left(\frac{M_{\text{BH}}}{10^7 M_{\odot}} \right)^{2.2} \left(\frac{V_{\text{ej}}}{10^3 \text{ km s}^{-1}} \right)^{-2.8} M_{\odot}, \quad (7)$$

where $\alpha \sim 0.1$ is the disk viscosity parameter, $\eta = (\epsilon_{\text{BH}}/0.1)(L_{\text{AGN}}/L_{\text{Edd}}) \sim 0.8$, and V_{ej} is the ejection velocity of the recoiled merged BH product. For high ejection velocities of $V_{\text{ej}} \gtrsim 1000 \text{ km s}^{-1}$ (e.g Hoffman & Loeb 2006) the latter relation yields the stringest constraints on the maximum disk mass that can be carried off by the recoiling black hole, namely $M_{\text{disk}} \lesssim 2 \times 10^6 [M_{\text{BH}}/(10^7 M_{\odot})]^{2.2} M_{\odot}$. The latter comfortably encompasses the estimated $M_{\text{AGN}}(\text{H}_2)$, making the presence of such a gas mass around the QSO consistent with an ejection scenario, provided that $M_{\text{BH}} > 10^7 M_{\odot}$.

5.2. The origin of the radio continuum

The system’s radio continuum was imaged by Feain et al. (2007) and consists of low-luminosity jets emerging from a radio-quiet core located at the QSO position. An important question arising from that study is how could the location of the HE 0450-2958 system near the FIR/radio correlation be explained if the starburst occurs in the companion galaxy while most of the radio emission is of AGN origin. Clues about a possible answer may be offered by the case of 1821+643, another radio-quiet but IR and optically luminous QSO ($M_V \sim -28$, $L_{\text{FIR}} \sim 9 \times 10^{12} L_{\odot}$) residing in a giant elliptical. This was the first radio-quiet QSO discovered to have classic FR I radio structure with low brightness diffuse jets (Papadopoulos et al. 1995), and a high brightness temperature compact core (Blundel et al. 1996), indicative of a black hole-based central engine. Despite the obvious AGN contribution in its radio continuum it did not deviate decisively from the far-IR/radio correlation until the discovery of a larger, 300 kpc-sized, low-brightness FR I radio structure (Blundell & Rawlings 2001). A similar scenario may apply in HE 0450-2958 and thus radio continuum imaging of this enigmatic system with good brightness sensitivity are urgently called for.

Interestingly, FR I-type radio structures may originate from a precessing jet axis due to binary black holes that have yet to coalesce (Blundel & Rawlings 2001). Such binaries, residing in gas-poor ellipticals (which allows for their long survival against gas-dynamical friction), are a fundamental prerequisite in the scenario of ejected AGNs as the outcome of a three-body kick during gas-rich/gas-poor galaxy interactions (Hoffman & Loeb 2006).

6. Gas-rich/gas-poor galaxy interactions misidentified?

The discovery of large dust and molecular gas reservoirs in *optically* selected QSOs where they fuel intense starbursts (e.g. Alloin et al. 1992; Haas et al. 2000; Evans et al. 2001; Bertram et al. 2007), solidified the AGN-starburst link found by other studies (e.g. Canalizo & Stockton 2001), with the dynamical interaction being the likely trigger for both activities. However, the exact nature of the QSO’s host galaxy in HE 0450-2958 aside, its difficult decomposition as an interaction between a gas/dust-poor galaxy (marked by a residing unobscured optically powerful QSO), and a gas-rich extreme starburst raises the possibility of *such interactions being misclassified as ULIRG→QSO transition objects*, in the standard ULIRG-to-QSO evolutionary picture.

In the latter picture interactions/mergers of progenitors with similar H_2 gas masses are involved, with an AGN always well within the interaction-induced starbursts (e.g. Sanders & Ishida 2004). Indeed, while such IR-warm galaxies with AGNs located amidst gas-rich starbursts are known (e.g. Bryant & Scoville 1999; Schinnerer et al. 1998; Evans et al. 1999), most studies lack the demanding combination of observational tools it took to reveal the true nature of HE 0450-2958. In fact without, a) HST imaging and a specialized deconvolution technique allowing sensitive probing of the host galaxy properties of an optically luminous QSO, and b) high resolution CO imaging with good S/N and excellent astrometry, the HE 0450-2958 system would have remained in the list of typical ULIRG→QSO transition objects. Current CO detections of ULIRGs and QSOs (e.g. Alloin et al. 1992; Evans et al. 2001; Scoville et al. 2003; Bertram et al. 2007) lack the good resolution/astrometry and/or high S/N to pinpoint a gas-rich starburst with respect to an optically luminous AGN even in the local Universe. Indicative of these limitations is PDS 456, the most luminous QSO in the local Universe (and another QSO/ULIRG composite in terms of its SED), where despite sensitive high resolution optical and CO imaging observations, the type of the QSO host and the location of the molecular gas with respect to the AGN remain unclear (Yun et al. 2004).

Thus, while the presence of large gas and dust reservoirs fuelling starbursts in optically selected luminous QSOs is now on firm statistical ground (e.g. Haas et al. 2000; Bertram et al. 2007), *it is far from certain that this rules out normal gas-poor elliptical galaxies as the hosts of optically powerful QSOs*, as is often stated (e.g. Scoville et al. 2003). Indeed, since little gas is needed to fuel an AGN, a merger of two gas-rich galaxies is not necessary. Instead a strong gas-rich spiral/gas-poor elliptical galaxy interaction can trigger a far-IR luminous starburst in the former and an optical/mid-infrared luminous AGN in the latter, with the composite IR/optical SED looking exactly like that of a typical warm ULIRG/QSO.

Finally, since the merger outcome of two gas-rich spiral disk progenitors is usually an elliptical (e.g. Barnes & Hernquist 1992 and references therein) it follows that, after a short

early epoch of mostly gas-rich mergers of disks, spiral/elliptical galaxy mergers would be frequent in the Universe. Recent numerical studies of such events by Di Matteo et. al. (2007) have demonstrated their ability to “ignite” short-lived starbursts. The latter, along with the activation of an optically luminous AGN in the gas/dust-poor elliptical progenitor, provide the luminous characteristic “beacons” marking such interactions. The so-called ULIRG→(optical QSO) transition objects are an excellent place to start their study.

7. Conclusions

We performed CO line emission imaging observations of the enigmatic QSO/galaxy pair HE 0450-2958 using the ATCA (CO J=1–0) and the SMA (CO J=3–2) detecting the J=1–0 line, our conclusions are as follows,

1. The CO J=1–0 line emission is associated with the companion galaxy not the QSO, and corresponds to $M_{\text{gal}}(\text{H}_2) \sim (1-2) \times 10^{10} M_{\odot}$, setting this galaxy on par with the most gas-rich ULIRGs in the local Universe, and solidifying the interacting status of this galaxy/QSO pair.
2. This molecular gas reservoir is distributed over an area of $\sim 10.7 \text{ kpc} \times 6.4 \text{ kpc}$, and amounts to $\gtrsim 30\%$ of the enclosed dynamical mass (assuming a rotationally supported disk). It fuels extreme star formation at a rate of $\sim 370 M_{\odot} \text{ yr}^{-1}$ and efficiencies of $L_{\text{IR}}/M(\text{H}_2) \sim (90 - 165) M_{\odot}/L_{\odot}$, typical for ULIRGs.
3. No molecular gas is detected towards the QSO itself with $M_{\text{QSO-host}}(\text{H}_2)/M_{\text{gal}}(\text{H}_2) \leq 1/5$, consistent with the little dust extinction or star formation activity deduced for its putative host galaxy. This weakens the case for a Narrow Line Seyfert 1 as the host galaxy since these are gas-rich spirals with luminous starbursts, and makes HE 0450-2958 a rare case of a gas-rich extreme starburst and a powerful QSO, intimately linked (via a strong interaction), but not coincident.
4. Most of radio continuum and the low-brightness jets of this system is due to AGN rather than star formation activity, and is typical for optically luminous but radio quiet QSOs with classical FR I structures residing in elliptical galaxies. Deeper radio continuum imaging of HE 0450-2958 with high brightness sensitivity and resolution is needed to verify this picture.
5. Given the early prominence of HE 0450-2958 as an IR-selected QSO exemplifying the ULIRG→(optical QSO) transition in a popular evolutionary scenario linking these classes, its hereby revealed nature as a strong interaction of a gas-rich and a gas-poor (yet to be identified) elliptical galaxy opens up the possibility that some of these so-called transition objects are such interacting pairs instead. There an interaction-induced starburst in the gas-

rich progenitor and a similarly activated optically luminous AGN in the gas-poor one will present a composite dust continuum typical of IR-warm ULIRG→QSO transition objects. Sensitive high resolution optical and CO imaging present the key for revealing such gas-rich/gas-poor galaxy dynamical interactions.

8. Acknowledgments

Jeff Wagg is grateful for support from the Max-Planck Society and the Alexander von Humboldt Foundation. We thank all the people that operate and maintain ATCA and in particular its 3 mm receivers for their dedicated support. Padelis Papadopoulos is grateful to Karl Jesienowski aboard the *Undersea Explorer* for fruitful conversations, and acknowledges Marcella Carollo for bringing this controversial object to his attention. Last but not least he would like to thank Margarita Zakalkas for inspiration during his residence in Zurich. The Australia Telescope is funded by the Commonwealth of Australia for operation as a National Facility managed by CSIRO.

REFERENCES

- Aalto S., Booth R. S., Black J. M., & Johansson L. E. B. 1995, *A&A*, 300, 369
- Alloin D., Barvainis R., Gordon M. A., & Antonucci R. R. J. 1992, *A&A*, 265, 429
- Bahcall J. N., Kirhakos S., & Schneider D. P. 1994, *ApJ*, 425, L11
- Barnes J. E., & Hernquist L. 1992, *ARA&A*, 30, 705
- Bertram T., Eckart A., Fischer S., Zuther J., Straubmeier C., Wisotzki L., & Krips M. 2007, *A&A*, 470, 571
- Blitz, L. 1997, in *CO: Twenty-Five Years of Millimeter-Wave Spectroscopy*, IAU Symposium No. 170, pg. 11
- Blundell K. M., Beasley A. J., Lacy M., & Garrington S. T. 1996, *ApJ*, 468, L91
- Blundell K. M., Rawlings S. 2001, *ApJ*, 562, L5
- Bonning E. W., Shields G. A., & Salviander S. 2007, *ApJ*, 666, L13
- Boyce P. J., Disney M. J., Blades J. C., Boksenberg A., Crane P., Deharveng J. M., Macchetto F. D., Mackay C. D., & Sparks W. B. 1996, *ApJ*, 473, 760
- Bryant P. M., & Scoville N. Z. 1996, *ApJ*, 457, 678
- Bryant P. M., & Scoville N. Z. 1999, *AJ*, 117, 2632
- de Grijp M. H. K., Lub J., & Miley G. K. 1987, *A&AS*, 70, 95
- Canalizo G., & Stockton A. 2001, *ApJ*, 555, 719
- Devereux N., Taniguchi Y., Sanders D. B., Nakai N., Young J. S. 1994, *AJ*, vol. 107, no. 6, p. 2006-2016
- Di Matteo P., Combes F., Melchior A.-L., & Semelin B. 2007, *A&A*, 468, 61
- Downes D., Solomon, P. M. 1998, *ApJ*, 507, 615
- Evans A. S., Kim D. C., Mazzarella J. M., Scoville N. Z., & Sanders D. B. 1999, *ApJ*, 521, L107
- Evans A. S., Surace J. A., & Mazzarella J. M. 2000, *ApJ*, 529, L85
- Evans A. S., Frayer D. T., Surace J. A., & Sanders D. B. 2001, *AJ*, 121, 3286

- Evans A. S., Mazzarella J. M., Surace J. A. & Sanders D. B. 2002, *ApJ*, 580, 749
- Evans A. S., Solomon P. M., Tacconi L. J., Vavilkin T., & Downes D. 2006, *AJ*, 132, 2398
- Floyd D. J. E., Kukula M. J., Dunlop J. S., McLure R. J., Miller L., Percival W. J., Baum S., & O’Dea C. P. 2004, *MNRAS*, 355, 196
- Frayser D. T. et al. 1999, *ApJ*, 514, L13
- Haas M., Müller S. A. H., Chini R., Meisenheimer K., Klaas U., Lemke D., Kreysa E., & Camenzind M. 2000, *A&A*, 354, 453
- Haehnelt M. G., Davies M. B., & Rees M. J. 2005, *MNRAS*, 366, L22
- Helfer T. T., et al. 2003, *ApJS*, 145, 259
- Hoffman L., & Loeb A. 2006, *ApJ*, 638, L75
- Hutchings J. B., & Neff S. G. 1988, *AJ*, 96, 1575
- Feain I. J., Papadopoulos P. P., Ekers R., & Middelberg E. 2007, *ApJ*, 662, 872
- Floyd D. J. E., Kukula M. J., Dunlop J. S., McLure R. J., Miller L., Percival W. J., Baum S. A., O’Dea C. P. 2004, *MNRAS*, 355, 196
- Greve T. R., et al. 2005, *MNRAS*, 359, 1165
- Kim M., Ho L. C., Peng C. Y., Im M. 2007, *ApJ*, 658, 107
- Letawe G., Magain P., & Courbin F. 2007, *A&A* (in press), arXiv:0709.3743v1
- Loeb A. 2007, *Physical Review Letters*, 0031-9007/07/99(4)/041103(4)
- Low F. J., Cutri R. M., Huchra J. P., & Kleinman S. G. 1988, *ApJ*, 327, L41
- McLure R. J., & Dunlop J. S. 2002, *MNRAS*, 331, 795
- Magain P., Letawe G., Courbin F., Jablonka P., Jahnke K., Meylan G., & Wisotzki L. 2005, *Nature*, Vol. 437, 318
- Merritt D., Storchi-Bergmann T., Robinson A., Batcheldor D., Axon D., & Cid Fernandes R. 2006, *MNRAS*, 367, 1746
- Middelberg E., Sault R. J., & Kesteven M. J. 2006, *Publications of the Astronomical Society of Australia*, Vol. 23, Issue 4, p. 147

- Papadopoulos P. P., Seaquist E. R., Wrobel J. M., & Binette L. 1995, *ApJ*, 446, 150
- Planesas P., Scoville N. Z., & Myers S. T. 1991, *ApJ*, 369, 364
- Regan W. M., et al. 2001, *ApJ*, 561, 218
- Sanders D. B., et. al. 1988, *ApJ*, 328, L35
- Sanders D. B., Scoville N. Z., & Soifer B. T. 1991, *ApJ*, 370, 158
- Sanders D. B., & Ishida C. M. 2004, in *The Neutral ISM in Starburst Galaxies*, ASP Conference Series, Vol. 320, pg. 230
- Schinnerer E., Eckart A., & Tacconi L. J. 1998, *ApJ*, 500, 147
- Schinnerer E., Eckart A., & Tacconi L. J. 1999, *ApJ*, 524, L5
- Scoville N. Z., Frayer D. T., Schinnerer E., & Christopher M. 2003, *ApJ*, 585, L105
- Scoville N. Z. 2004, in *The Neutral ISM in Starburst Galaxies*, ASP Conference Series, Vol. 320, pg. 253
- Solomon P. M., Downes D., Radford S. J. E., & Barrett J. W. 1997, *ApJ*, 478, 144
- Staguhn J. G., Schinnerer E., Eckart A., & Scharwächter J. 2004, *ApJ*, 609, 85
- Tacconi L. J., Genzel R., Blietz M., Cameron M., Harris A. I., & Madden S. 1994 *ApJ*, 426, L77
- Yao L., Seaquist E. R., Kuno N., & Dunne L. 2003, *ApJ*, 588, 771
- Yun M. S., Reddy N. A., Scoville N. Z., Frayer D. T., Robson E. I., & Tilanus R. P. J. 2004, *ApJ*, 601, 723

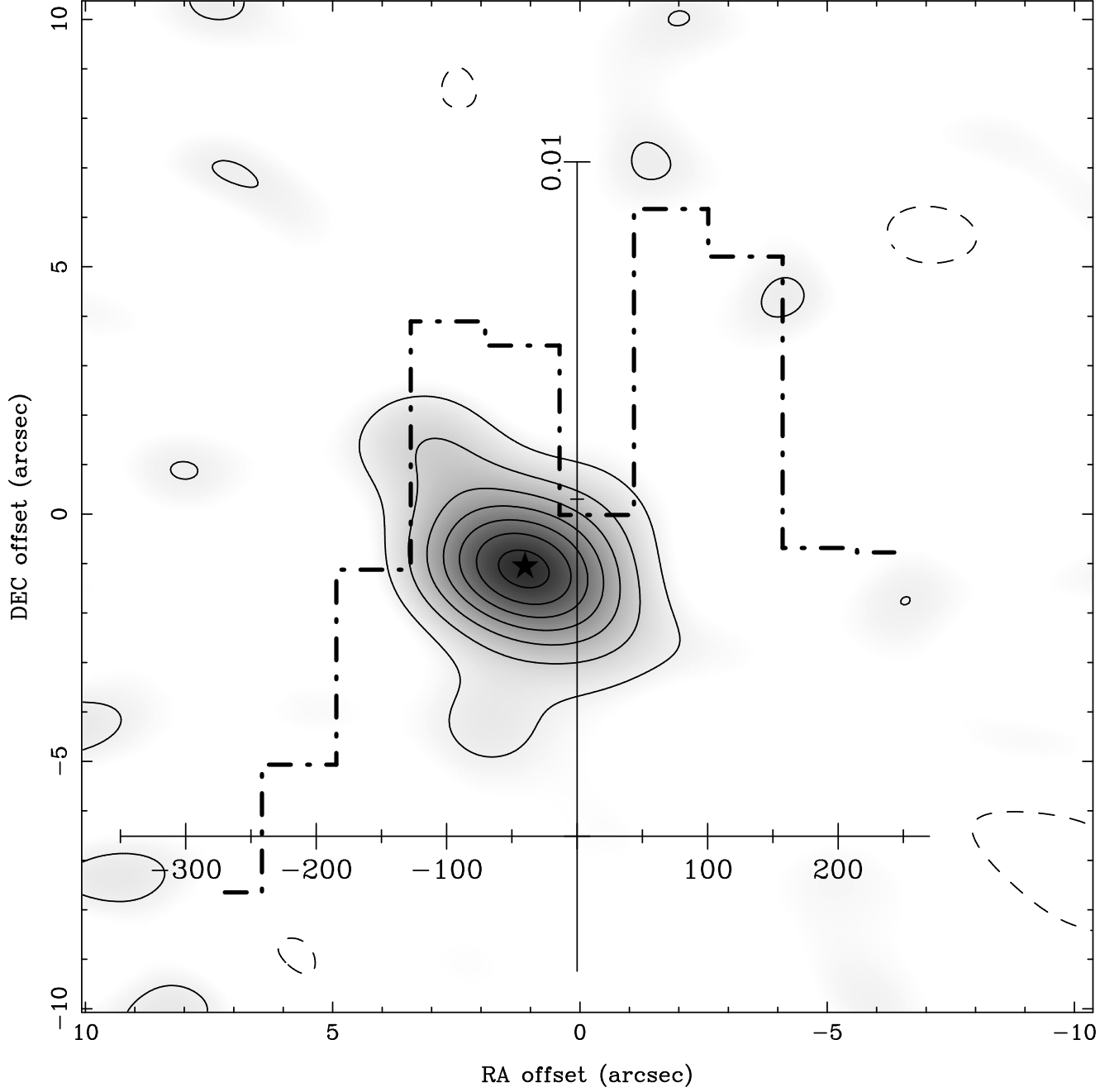


Fig. 1.— Map of CO J=1–0 emission (CLEANed, NA-weighted), averaged over the IF1+IF2 band, with $\Theta_{\text{beam}} = 3.21'' \times 2.14''$, $\text{PA} = 72^\circ$ (Section 3.1), contours: $(-2, 2, 4, 6, 8, 10, 12, 14) \times \sigma_{\text{rms}}$ where $\sigma_{\text{rms}} = 0.45 \text{ mJy/beam}$. The phase center ($0'', 0''$) corresponds to the QSO’s radio core position: $\alpha_{\text{core}} = 04^{\text{h}} 52^{\text{m}} 30^{\text{s}}.1$, $\delta_{\text{core}} = -29^\circ 53' 35.0''$ (Feain et al. 2007). The overlaid spectrum corresponds to the peak CO emission (marked with a star), located at $(\Delta\alpha, \Delta\delta) = (1.15'', -1.05'')$ away from QSO’s radio core.

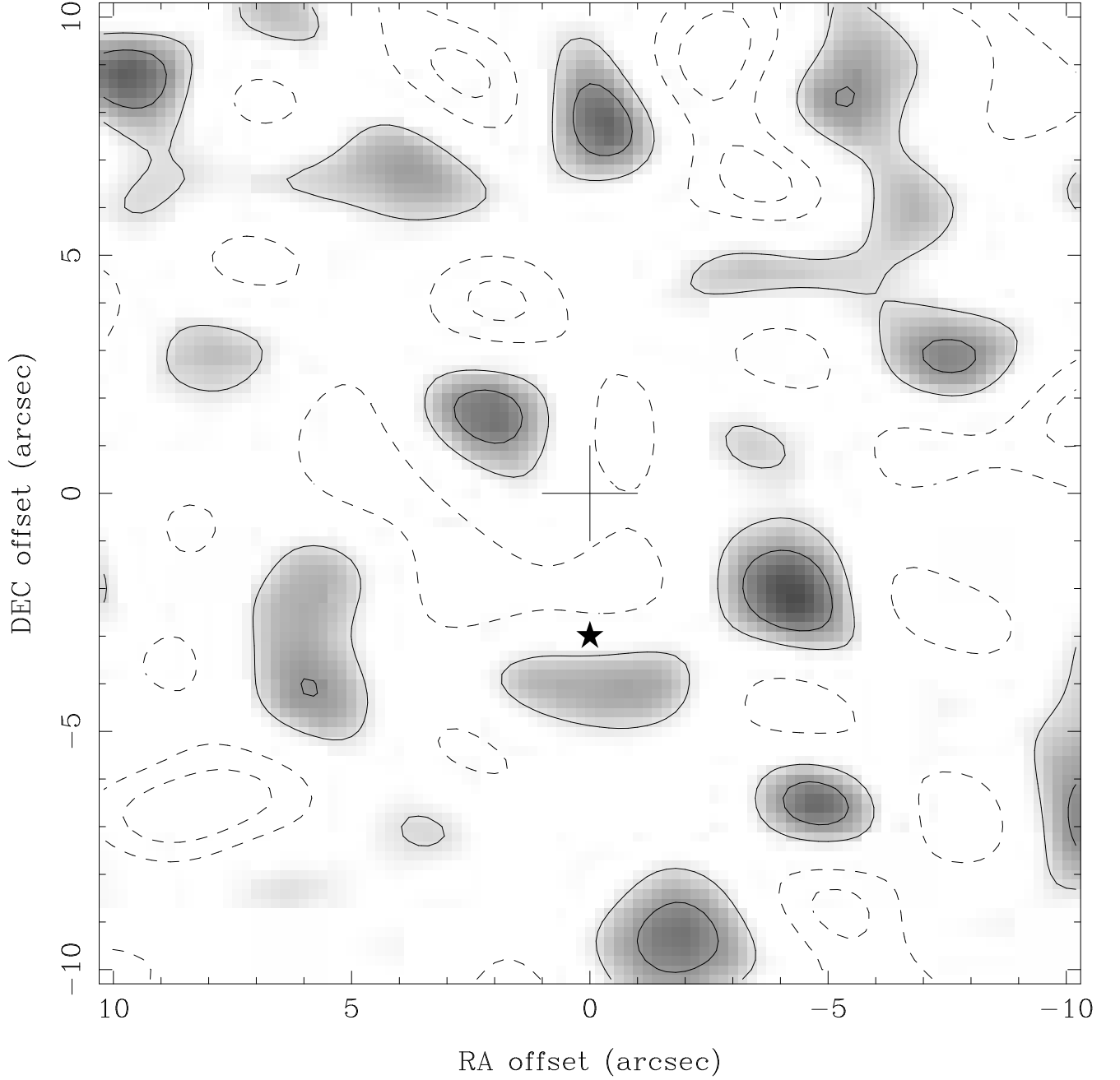


Fig. 2.— Map of mm continuum emission at 94.53 GHz (NA-weighted), averaged over the IF1+IF2 band, with $\Theta_{\text{beam}} \sim 2.85'' \times 1.70''$, PA = 67° (Section 3.1), contours: $(-1, 1, 2) \times \sigma_{\text{rms}}$, where $\sigma_{\text{rms}} = 0.5 \text{ mJy/beam}$. In these observations the phase center ($0'', 0''$) (marked by the cross), is placed $\sim 3''$ to the north of the QSO's radio core (marked now by a star) to avoid residual correlator offset effects (see Section 2). No emission is detected at the position of the QSO with a limit of $S_{94.5 \text{ GHz}} \leq 1.5 \text{ mJy/beam}$ (3σ).

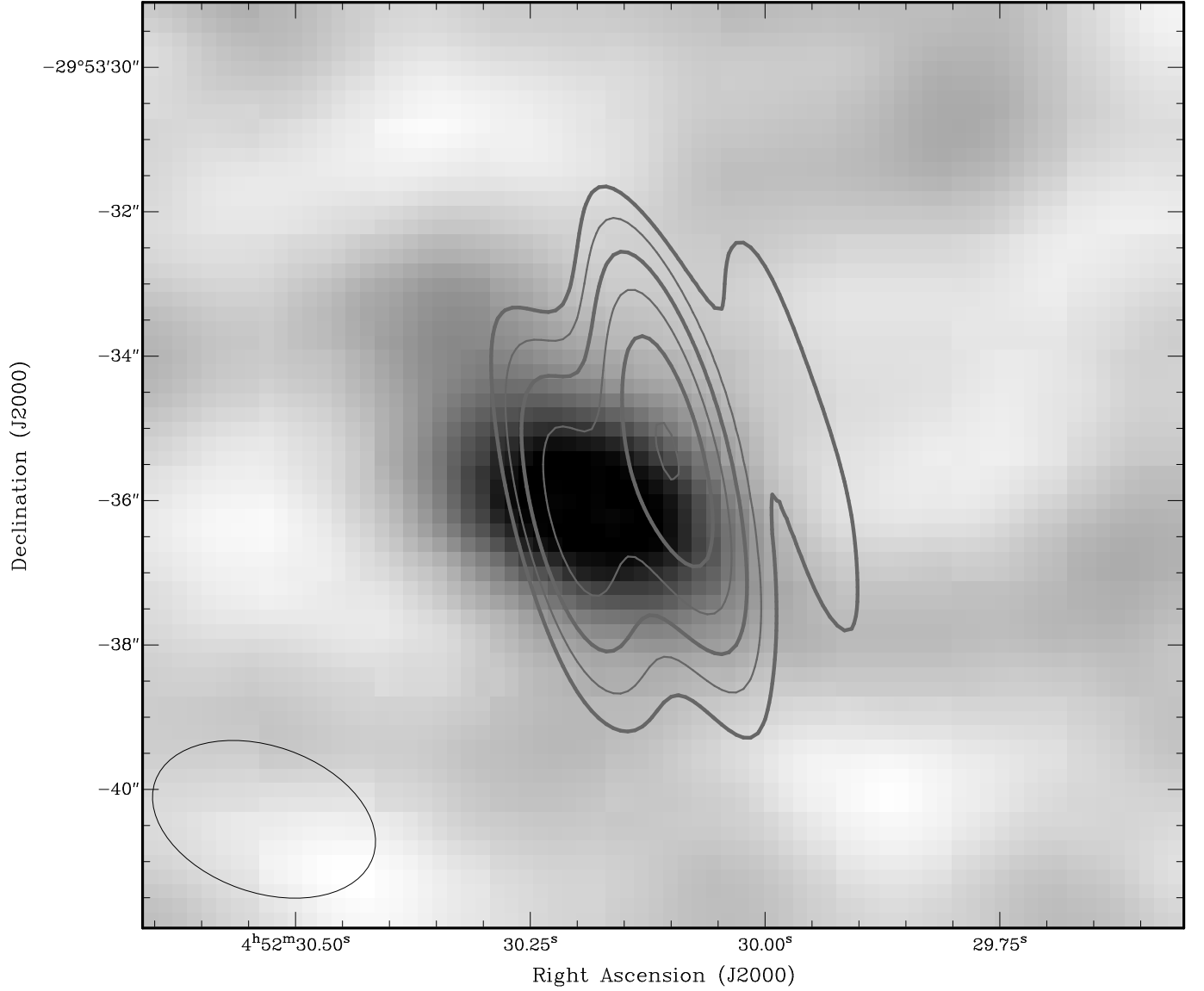


Fig. 3.— ATCA CO(1-0) greyscale image with ATCA 8.4GHz radio continuum contours overlaid. Contour levels start at $200\mu\text{Jy beam}^{-1}$ and increase in a geometric series with a common ratio of $\sqrt{2}$. The size of the CO(1-0) synthesised beam is shown in the bottom left corner of the image.

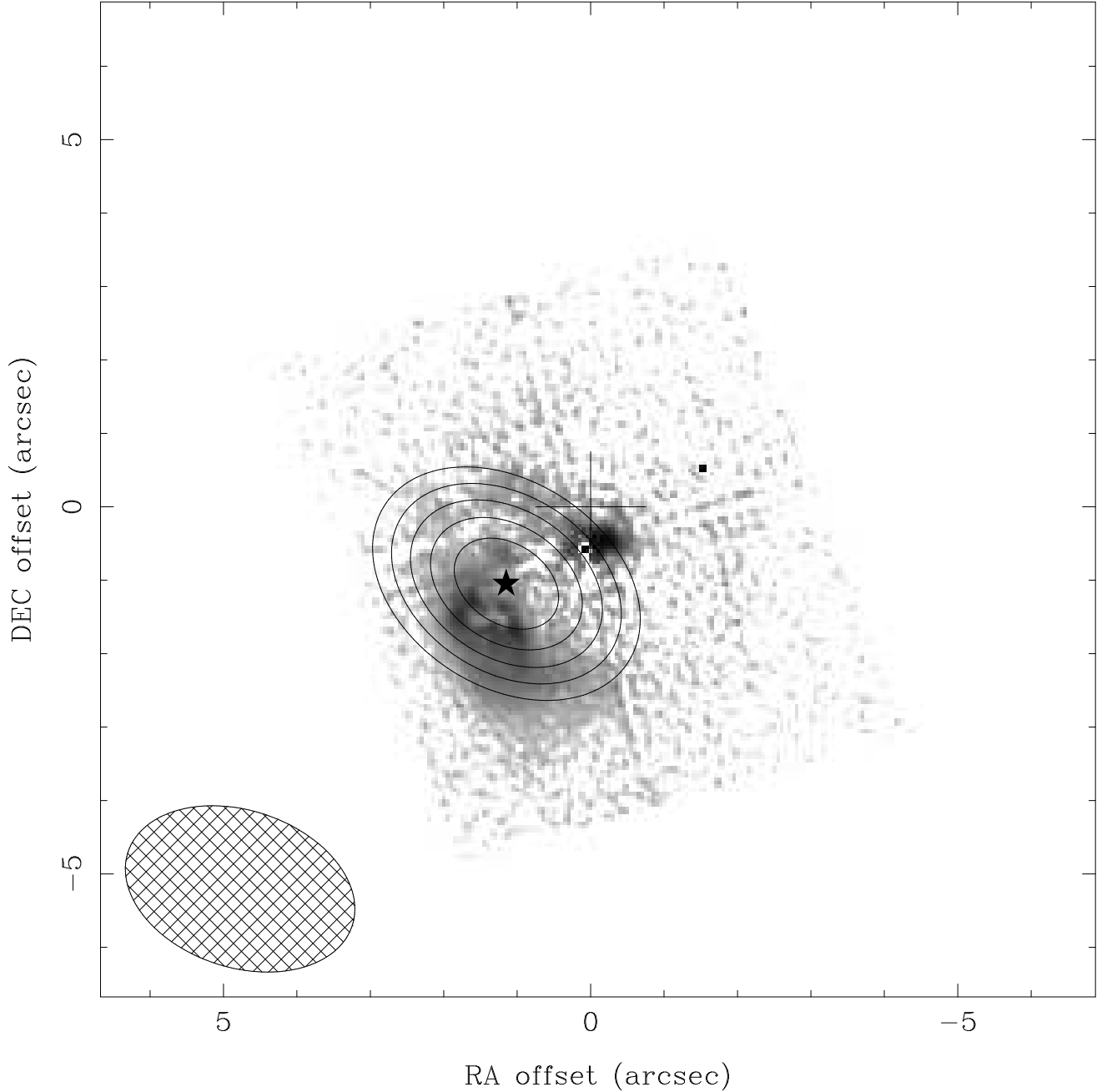


Fig. 4.— The CO J=1–0 deconvolved source model ($2.5'' \times 1.5''$, $\text{PA} = 35^\circ \pm 10^\circ$, see text) overlaid on the HST/ACS deconvolved image of HE 0450-2958 (contours: 50% \rightarrow 100% in steps of 10% of the peak), where the QSO contribution has been carefully subtracted (adapted from Magain et al. 2005). The ATCA beam ($\Theta_{\text{beam}} = 3.21'' \times 2.14''$, $\text{PA} = 72^\circ$) is shown at the bottom left. In the HST image the QSO is marked by the single bright pixel near the phase center ($0'', 0''$) denoted by a cross (and placed at AGN’s radio core). The AGN-excited gas cloud near the AGN’s position and the IR-luminous starbursting companion galaxy are clearly discernible. The HST astrometric uncertainties ($\sim 0.5'' - 1''$), denoted by the size of the cross marking the phase center are the dominant ones (Section 3.1). A $\sim 0.7''$ northward shift of the optical image aligning radio and optical AGN positions brings the CO source exactly on top of the companion galaxy).

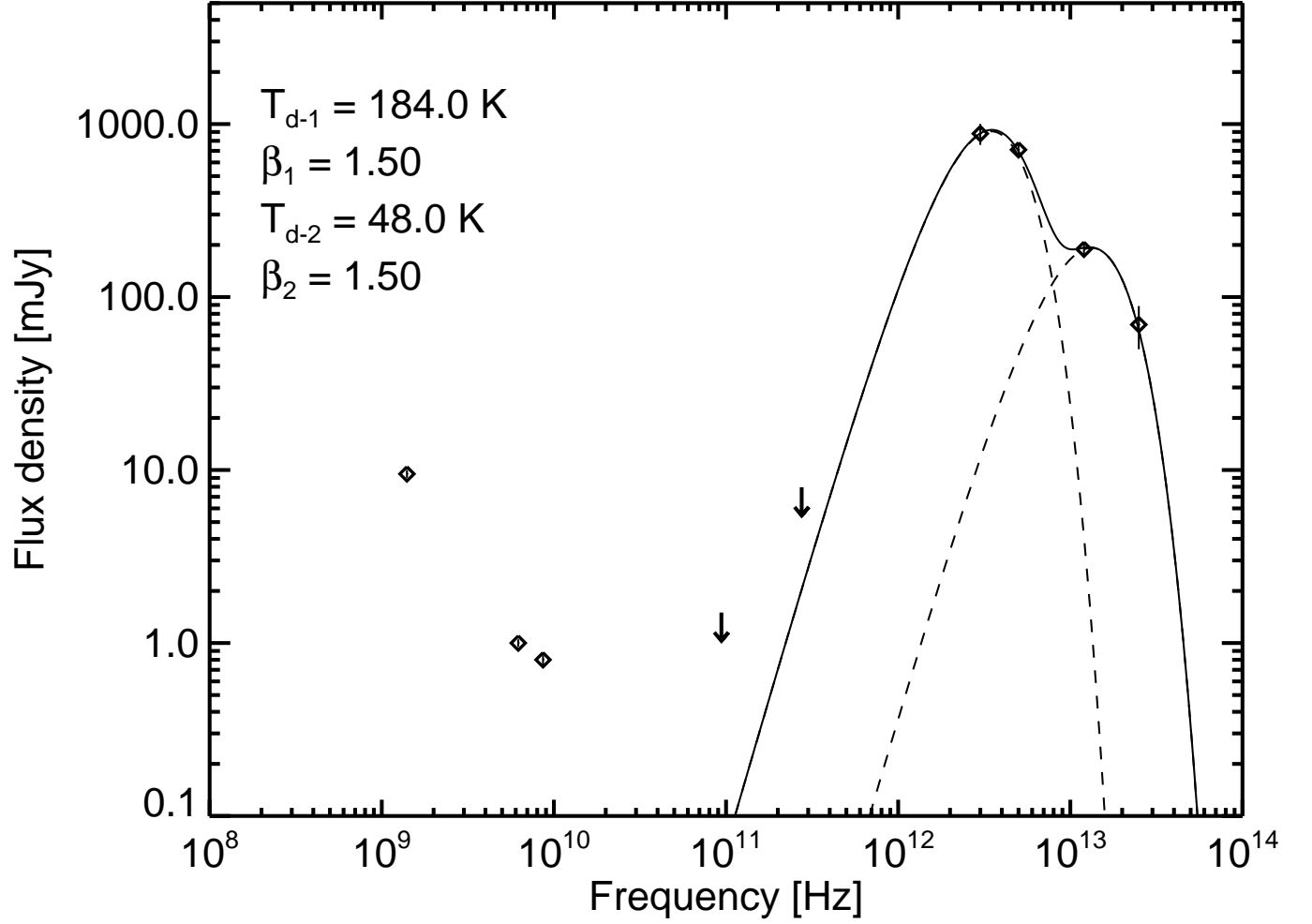


Fig. 5.— Two component fits of the mm/IR dust continuum of HE 0450-2958. The upper limits at mm wavelengths were obtained from this work, the IR data are IRAS fluxes at $12 \mu\text{m}$, $25 \mu\text{m}$, $60 \mu\text{m}$, and $60 \mu\text{m}$.